Identification of self-discharge mechanisms of ionic liquid electrolyte based supercapacitor under high-temperature operation

Journal of Power Sources 485 (2021) 229328

Contents lists available at ScienceDirect

Journal of Power Sources

journal homepage: www.elsevier.com/locate/jpowsour

Identification of self-discharge mechanisms of ionic liquid electrolyte based supercapacitor under high-temperature operation

Mazharul Haque [a,*], Qi Li [a,b], Cristina Rigato [c], Azega Rajaras [a,b], Anderson D. Smith [a], Per Lundgren [a], Peter Enoksson [a,b]

[a] Micro and Nanosystems Group, Department of Microtechnology and Nanoscience, Chalmers University of Technology, 412 96, Gothenburg, Sweden
[b] Wallenberg Wood Science Center, Chalmers University of Technology, 41296, Gothenburg, Sweden
[c] Chalmers University of Technology, 41296, Gothenburg, Sweden

HIGHLIGHTS

- Self-discharge mechanisms of ionic liquid-based supercapacitors are identified.
- Voltage decay is dependent on the instant temperature rather than former exposure.
- Contributions from charge redistribution and diffusion are seen at high voltage.
- The diffusion mechanism dominates at low voltage and high temperature.
- The decreased RC time constant at high temperature affects self-discharge behaviour.

ARTICLE INFO

Keywords:
Supercapacitor
Self-discharge
Leakage current
High temperature
Ionic liquid
Activated carbon

ABSTRACT

Ionic liquids (ILs) are promising electrolytes for supercapacitors (SCs) aimed for high-temperature applications, where increased ionic conductivity results in superior capacitive performance compared to room temperature (RT) performance. However, an increased temperature also accelerates the self-discharge rate that adversely affects energy retention and restricts the usage of SCs in standalone applications. In this study, a detailed electrochemical investigation on the self-discharge behaviour of carbon-based SCs containing an IL, 1-Ethyl-3-methylimidazolium acetate (EMIM Ac), has been carried out in the temperature range RT - 60 °C, and the underlying self-discharge mechanisms are identified. The results reveal that at a high voltage of 1.5 V, the self-discharge is characterized by a combination of charge redistribution and diffusion at both RT and 60 °C. At 60 °C, the diffusion-controlled mechanism dominates at lower voltages over the charge redistribution effect, while at RT both mechanisms contribute to a similar extent. The observed difference in the self-discharge mechanism between RT and 60 °C is explained in terms of a decreased RC time constant (τ_{RC}) at elevated temperature, and the same conclusions are potentially applicable to other IL-containing SCs as well.

1. Introduction

Supercapacitors (SCs) are known to be efficient energy storage devices with a very high power density and long cycle life owing to their intrinsic electrostatic charge storage mechanism (for electrical double layer type SCs). Despite their advantageous properties, applications are somewhat limited because of their inferior energy density and high self-discharge rate as compared to batteries [1–3]. Over the years, a significant research effort has been directed towards increasing the energy density by utilizing novel electrolytes with high operating voltages [4–9], electrodes with high capacitance [10–13], or hybrid devices containing both capacitive and battery-type electrodes [14–17]. However, the issue related to self-discharge remains an obstacle to implementing the SCs in numerous applications, especially where frequent recharging is not available, and when the devices are required to stay in a charged state for an extended period of time [18]. Self-discharge is a spontaneous voltage drop of the electrochemical devices from a charged state when not connected with any load. The energy is proportionally

* Corresponding author.
E-mail address: mhaque@chalmers.se (M. Haque).

https://doi.org/10.1016/j.jpowsour.2020.229328
Received 4 August 2020; Received in revised form 29 October 2020; Accepted 2 December 2020
Available online 16 December 2020

related to the square of the voltage; therefore, the voltage loss caused by self-discharge has a negative influence on the overall performance of the device [19].

The voltage decay due to self-discharge is attributed to the mechanisms identified by Conway et al. [2], namely ohmic leakage, activation- and diffusion-controlled mechanisms, and charge redistribution (CR) inherent to porous carbon electrodes proposed by Levie et al. [20]. The mathematical expression of the voltage decay of the representative mechanisms can be found in section 2.3. The self-discharge due to ohmic leakage is more relevant to the conventional dielectric capacitors, where the voltage loss is an electric field driven process occurring within the system with flat metal plates and does not involve any ions or complex porous structure that are part of SCs [21]. Typically, this kind of self-discharge occurs due to an undesired faulty construction of devices that creates a conductive pathway between the electrodes [2].

The activation-controlled self-discharge occurs because of the Faradaic reactions due to overcharging. When a high concentration of electroactive species exists in the device, overcharging beyond the electrolyte decomposition voltage limit [22] or the potential of oxidation/reduction originating from the surface functional groups will result in self-discharge [23] that kinetically follows the Tafel equation. The diffusion-controlled self-discharge corresponds to the oxidation/reduction reactions originating from the presence of a low concentration of impurities (for instance, transition metal ions like Fe^{3+}, Fe^{2+}, adsorbed oxygen in carbon materials or electrolyte contaminants) that are electroactive within the voltage limit [24–26]. Therefore, the self-discharge rate relies on the transport or diffusion of these species to or from the electrode surface. Fick's law of diffusion models the dynamics of the potential decay of planar electrodes, related to semi-infinite diffusion. In porous electrodes, the diffusion mechanism was found to be similar to planar electrodes [27]. A related diffusion-controlled model was developed for full cell SCs by B.W. Ricketts and C. Ton-That [21]. In this case, the diffusion process was originating from an accumulation of excess ionic concentration near the electrode surface, and the voltage in the self-discharge profile declined linearly with the square root of time within an initial relatively short period.

Lastly, CR is recognized to be the main reason for the voltage decay of SCs containing carbon electrodes [18,28–30]. Inherent characteristics of carbon electrodes with diverse pore shape, size, and distribution result in limitations of the migration of electrolyte ions and create inequality in charging rates, where pores with different geometries are charged at different rates [20,31]. CR can be described by a transmission line model, where charging different pores is analogous to charging different RC (resistor/capacitor) subsystems with different time constants (τ_{RC}), which results in a nonequilibrium charged state [32]. Under the open-circuit condition, CR drives the nonequilibrium charged state towards equilibrium by synchronizing the charges from a higher to a lower surface charge density. Consequently, an apparent voltage decay is observed. The self-discharge profile due to CR can exhibit different shapes based on the rate-limiting process (resistance-limited or diffusion-limited), or based on the surface potential (higher or lower compared to the bulk) [18,27,33].

In order to efficiently suppress the self-discharge, one essential step is to identify the underlying self-discharge mechanism so that necessary actions can be taken to modify the components of the device accordingly. To date, most studies are limited to aqueous [34–41] and organic electrolyte-based systems [21,42–44]. However, a few studies have reported the self-discharge behaviour of ionic liquid (IL)-based systems. IL electrolytes are a promising alternative to traditional aqueous and organic electrolytes, owing to their high electrochemical stability with a wide operating voltage window [45]. Furthermore, they are particularly suitable for high-temperature applications because of their high thermal stability. Previous studies have demonstrated that SCs containing IL electrolytes reach their optimal electrochemical performance at a temperature of around 60 °C [46]. However, when operating at high temperatures, there is a greater risk for an unpredictable behaviour of the device due to the influence of temperature variation on the self-discharge mechanisms. Roughly, the rate of self-discharge current doubles for every 10 K increase in temperature [47].

Among the few reported studies on self-discharge of IL-containing SC, Norihisa et al. [48] reported the self-discharge behaviour of imidazolium-based ILs. The observed voltage loss of IL-based devices was shown to be less significant than the voltage loss of a device containing conventional organic electrolyte, and it was attributed to the higher viscosity of the ILs. Ann et al. [49] reported that self-discharge and leakage current analysis could be used as a quick measure of the long-term stability of IL-based SCs. They showed that the self-discharge of imidazolium-based IL containing SCs exhibits a faster rate with carbon electrodes containing a higher amount of mesopores than micropores. The underlying self-discharge mechanisms were associated with both CR and Faradaic reactions. However, there was no investigation of the high-temperature influence on the self-discharge mechanisms, despite high-temperature compatibility being one of the strong driving forces to use the IL in the first place. Francesca et al. [50] showed that the SCs containing pyrrolidinium-based ILs are less affected by self-discharge compared to SCs containing conventional organic electrolyte (propylene carbonate solvent)-based SCs. A general trend of increasing leakage current and self-discharge rate was observed with increasing temperature (up to 60 °C). However, there was no explanation of possible self-discharge mechanisms behind the observed self-discharge profile.

In this regard, a systematic analysis of the underlying self-discharge mechanisms of IL electrolyte-based SCs is needed in order to predict the reliability at elevated temperatures and to identify potential countermeasures. Previously [51], a thorough electrochemical investigation was carried out on a SC containing an IL electrolyte, 1-Ethyl-3-methylimidazolium acetate (EMIM Ac) with 10 wt% water, in a wide temperature range. Generally, ILs are more viscous compared to conventional organic or aqueous electrolytes due to the bulky nature of ions and absence of any solvent. They tend to form aggregates due to high ionic association and exhibit quite high equivalent series resistance (ESR) that adversely affects the capacitive performance and power density. $[EMIM]^+$ cation-based IL possess a relatively high ionic conductivity (10 mS cm^{-1}) compared to most other ILs. Although the presence of water restricts the operating voltage window to be 1.5 V, it does improve the ionic dissociation by reducing the direct coulombic interaction between the anions and cations, which results in even higher ionic conductivity. Owing to the enhanced mobility of electrolyte ions, the device delivered excellent capacitive performance up to 150 °C. As a continuation of the previous study, the current study aims at revealing the underlying self-discharge mechanisms of SCs containing an IL electrolyte (EMIM Ac) at different temperatures, ranging from RT to 60 °C.

2. Experimental

2.1. Materials

The main component of the electrodes was activated carbon (AC), (Kuraray®, YP-80F). As a first step, the AC powder and carbon black (Sigma Aldrich) were mixed and finely ground in a quartz mortar. Afterward, the mixture was poured into a beaker containing acetone and polytetrafluoroethylene (PTFE) binder (60 wt% in H_2O) in a weight ratio of 80:10:10 in the respective order of AC powder, carbon black and PTFE. Later the mixture was kept in sonication for 30 min and subsequently transferred to a water bath of 75 °C for solvent (acetone) evaporation. Consequently, a dough was obtained from the mixture and processed into a freestanding film by a rolling press technique. Then the film was dried in vacuum for 24 h at 80 °C. Afterward, several pellets with a 10 mm diameter were punched out from the dried film and used as electrodes. The electrodes were around 3.18 mg cm^{-2} in mass loading (2.5 mg in mass with a geometrical area of 0.785 cm^2), and 100 μm in

thickness. The surface area of the as-prepared AC electrode (80% YP-80F AC, 10% PTFE, and 10% carbon black) and AC powder (Kuraray®, YP-80F) is calculated to be 1565 ± 30 m^2g^{-1} and 2028 ± 24 m^2g^{-1}, respectively, with an even distribution of micropores and mesopores. As can be seen from Fig. S1 the ESCA (electron spectroscopy for chemical analysis) demonstrates that the prepared electrode materials contained 94.1 at.% carbon along with 5.90 at.% oxygen. The resolved peaks from the spectra confirm the presence of some acidic surface oxygen functional groups such as C–O (phenols and ethers), C═O (carbonyl), O–C═O (carboxyl, lactones). The detailed electrode material characterizations regarding surface morphology, surface area, and thermal stability are reported in a previous article [51].

Commercially available glassfiber sheets (GF, Whatman®) with 200 μm thickness and a diameter of 16 mm were used as the separator.

1-Ethyl-3-methylimidazolium acetate 97% (EMIM Ac, Sigma Aldrich) was used as an electrolyte solution without further purification. Thermogravimetric analysis of the pristine EMIM Ac electrolyte and a mixture of EMIM Ac and AC electrode revealed the presence of around 10 wt% of water. A detailed measurement protocol and the analysis of the result is reported in the previous article [51].

2.2. Device preparation

Symmetric two-electrode SC devices were prepared with CR 2025 coin cells consisting of a SS304 stainless steel casing, an O-ring seal, a stainless steel current collector, and a stainless steel spring spacer. In total, four devices, namely: device 1 (D_1), device 2 (D_2), device 3 (D_3), and device 4 (D_4), were assembled with the electrode, electrolyte, and separator as mentioned above. Approximately 100 μL of electrolyte was used in each device. All the devices were kept idle for 72 h before electrochemical measurements in order to provide enough time for electrolyte adsorption into the AC electrodes.

To examine the temperature influence and the operating history on self-discharge behaviour, a systematic measurement protocol regarding the temperature rise was assigned to the devices in the following manner: D_1 (RT/21 °C → 40 °C → 50 °C → 60 °C), D_2 (40 °C → 50 °C → 60 °C), D_3 (50 °C → 60 °C) and D_4 (60 °C). Elevated temperature exposure was achieved by placing the cell in a DZF-6020 oven (temperature fluctuation ±1 °C). Additionally, the temperature was monitored by a UT61B Modern Digital Multimeter coupled with a thermal sensor connected to the device. The accuracy of the sensor is ±1.2% in a temperature range of −40 to 1000 °C. Once the devices reached a pre-set temperature, they were maintained at that constant temperature for at least 4 h, which ensured that the critical dynamical processes within the devices could reach thermal equilibrium before self-discharge measurements were performed. Additionally, a single frequency (0.1 Hz) electrical impedance spectroscopy (EIS) was carried out during the whole period of 4 h with a time interval of 10 min to monitor the impedance behaviour of the devices while the temperature was rising to a pre-set value followed by thermal equilibrium. No significant change of the impedance characteristic at the end of the 4 h period further demonstrated that the devices under study reached thermal equilibrium.

2.3. Electrochemical measurements

The self-discharge behaviour of all the devices was characterized by employing an orderly electrochemical measurement as illustrated in the flowchart below (Scheme 1). Firstly, to assess the similarity of the electrochemical signature of the devices, the open-circuit voltage (V_{OC}) was monitored followed by an EIS measurement in a frequency range of 100 kHz to 10 mHz at a constant direct current (dc) voltage of 0 V with an alternating current (ac) perturbation of 10 mV. Then cyclic voltammetry (CV) was carried out from 0 to 1.5 V for 50 cycles with a scan rate of 20 mV s^{-1}. At the end of the cycling, the overlapping anodic and cathodic current from the forward and backward scan ensured a steady-state of the devices (Fig. S2).

After the pre-assessment, the devices were exposed to elevated temperatures. Upon reaching the pre-defined temperature with thermal equilibrium, they were galvanostatically charged to 1.5 V with a constant current of 50 mA g^{-1}. The devices were potentiostatically held at 1.5 V for 2 h to facilitate a more uniform CR among the pores of the electrodes. The leakage current data was collected from this step of the protocol. The devices were then disconnected from the power supply, and the self-discharge was recorded for 3 h by monitoring the V_{OC}. Afterward, the devices were galvanostatically discharged to 0 V with the

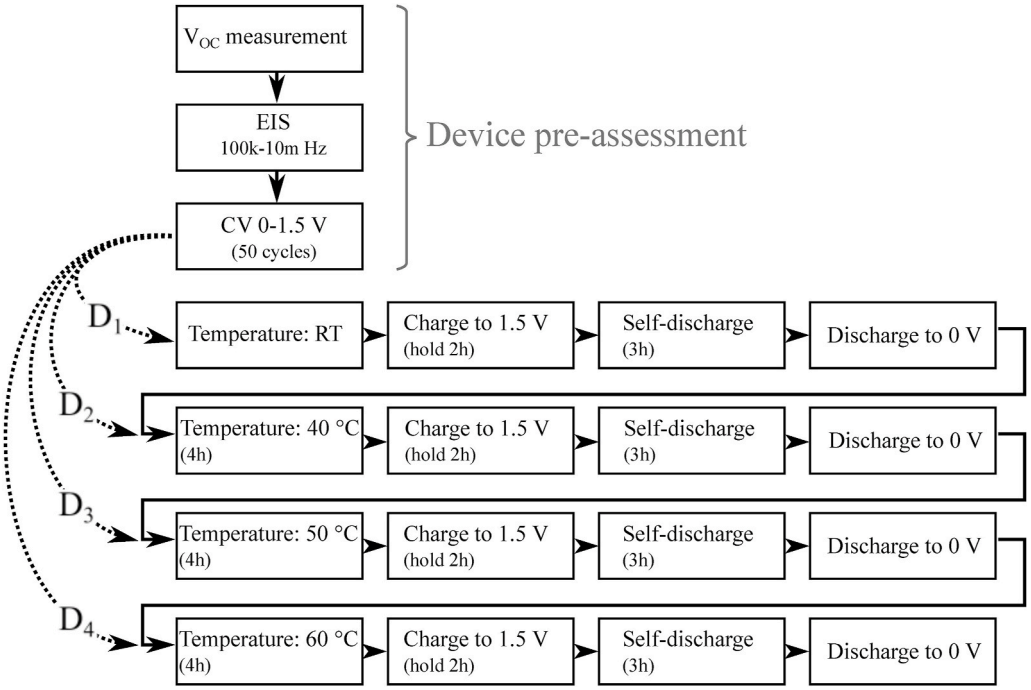

Scheme 1. Electrochemical measurement protocol with a systematic temperature exposure.

same constant current that was used during charging and conditioned for 2 h to ensure complete discharge. These measurement steps were followed for all the devices at each assigned temperature (as shown in the flow chart, Scheme 1) to investigate the temperature influence on the self-discharge behaviour.

Additional self-discharge measurements were conducted on D_4 at 60 °C and RT with different initial voltages (1.5, 1.4, 1.3, 1.2, 1.1, and 1.0 V) to verify and explore the self-discharge mechanisms occurring at respective voltages. These sets of measurements did not include any potentiostatic-holding step, and the self-discharge data was recorded for 1 h after galvanostatically charging with 50 mA g^{-1}.

All the measurements were conducted using a Gamry Reference 3000AE galvanostat/potentiostat workstation with an electrometer input impedance of >1014 Ω, current accuracy of (±10 pA, ± 0.3%) and voltage accuracy of (±1 mV, ±0.3%) of reading.

2.4. Self-discharge curve fitting

The mathematical representation of the proposed self-discharge mechanisms are as follows: Voltage loss due to ohmic leakage,

$$V = V_o\, e^{-t/RC} \tag{1}$$

where V_o is the initial voltage, C is the capacitance, R is the leakage resistance, and V is the voltage change over time (t).

Activation controlled self-discharge mechanism,

$$V = V_o - \frac{R_g T}{\alpha F} ln \frac{\alpha F i_o}{R_g T C} - \frac{R_g T}{\alpha F} ln\left(t + \frac{CK}{i_o}\right) \tag{2}$$

where R_g is the ideal gas constant, T is the temperature, α is the charge transfer coefficient, F is the Faraday's constant, i_o is the exchange current density, C is the interfacial capacitance, and K is an integration constant.

Diffusion controlled self-discharge mechanism,

$$V = V_o - \; C^{-1}\, 2zF{\cdot}AD^{\frac{1}{2}}\pi^{-\frac{1}{2}}\, c_o \sqrt{t} \tag{3}$$

where z is the charge number of the impurity ions, A is electrode surface area, D is a diffusion coefficient, and C_o is the initial concentration of impurities.

By combining equations (1)–(3), a general formula can be constructed as follows:

$$V = V_o\, e^{-t/RC} - B\sqrt{t} - m - n\, ln\left(t + \frac{CK}{i_o}\right) \tag{4}$$

where m and n are the constants correlated with the activation controlled mechanism, and B is correlated with the diffusion-controlled mechanism.

By discarding the ohmic leakage contribution, the relation between V and t can be written as

$$V = A - B\sqrt{t} - P\, ln(t + \tau) \tag{5}$$

where A, P, and τ are the parameters related to the Faradaic processes, and B is the diffusion parameter. It should be noted that the mathematical treatment of self-discharge caused by CR is regarded as the same as the activation controlled Faradaic process, i.e., equation (2). Therefore, the overall expression of equation (5) consists of contributions from CR and activation-controlled and diffusion-controlled Faradaic processes.

The self-discharge data fitting based on the activation/CR- and diffusion-controlled mechanisms was carried out with Python (Pandas library, scipy.optimize.curve_fit method). When fitting, the parameters (A, B, P, and τ) in equation (5) were constrained to be positive in order for the mathematical expression to be representative of the physics behind the self-discharge mechanism. In the fitting algorithm, the initial values of the four parameters were set to 0.86, 0.02, 0.11, 0.34, as found in Ref. [52]. The algorithm was also run several times with random initial values between 0.00 and 0.50 to rule out the possibility of local optimum, and the final result was unchanged.

3. Results and discussion

3.1. Temperature influence on self-discharge profile

Fig. 1(a) demonstrates the variation of the voltage loss of D_1 from an initial voltage of 1.5 V at different temperatures ranging from RT to 60 °C. It can be noticed that the magnitude of the self-discharge increases with elevated temperature. The accelerated self-discharge with increasing temperature is a well-known phenomenon observed in different studies [21,40,53,54] and generally occurs due to an enhanced electrochemical activity within the system.

However, the underlying mechanisms of the self-discharge could be different from system to system depending on electrode material, electrolyte, current collector, initial voltage, temperature, and charging history. The four representative primary mechanisms (ohmic leakage, activation-controlled, diffusion-controlled, and CR) of the self-discharge are expected to show distinct profiles and can be identified by different plotting procedures.

For instance, the self-discharge due to ohmic leakage exhibits a linear profile when plotted as the natural logarithm of voltage with time ($ln\ V$ vs t) and can be used as a sanity check for faulty construction of the device [2,27]. If the voltage loss is plotted against log (t) and the self-discharge profile follows a linear drop after an initial plateau, then the self-discharge rate-determining step can be related to an activation controlled mechanism [2,18]. Similarly, if the voltage loss is plotted against the square root of time ($t^{1/2}$) and there is a linear decline of voltage, then the rate-determining step is associated with the diffusion-controlled mechanism [2]. Voltage decay due to resistance-limited CR shows a similar profile as activation-controlled self-discharge, i.e., linear voltage drop when plotted against log (t). However, the slopes depend on the initial charging potential, unlike in the activation-controlled mechanism [18,30].

In this regard, to gain a better understanding and to identify the self-discharge mechanism in the current system, the voltage loss is plotted against log (t) and $t^{1/2}$, shown in Fig. 1(b) and Fig. 1(c), respectively. The plot of $ln\ V$ vs t did not exhibit the linear drop and was discarded as a potential reason behind self-discharge. Given that the contribution from ohmic leakage occurs when there is an unwanted conducting pathway between two electrodes; the obtained non-linear drop in voltage suggests that there is no fault in the construction of the device.

It can be seen from Fig. 1(b) that the self-discharge follows a linear drop after an initial plateau, which matches the characteristic profile of both the activation controlled and CR mechanism. The initial plateau at the short-time scale is typical and corresponds to τ in equation (5); it also involves the integration constant, K from equation (2). The length of the plateau provides critical mechanistic information regarding exchange current density or interfacial capacitance [2,18,27]. As seen in Fig. 1(b), the length of the initial plateau is decreasing with increasing temperature. For an activation-controlled mechanism, the plateau length is inversely related to the initial self-discharge current [2,33]. Therefore, a shorter plateau indicates an increased self-discharge current. Similarly, for a CR mechanism, the plateau length depends on the RC time constant (τ_{RC}), and a shorter plateau hints for a decreased τ_{RC} [28,55]. It can also be noticed that the voltage decline after the plateau is increasing with increasing temperature. Consequently, the slope of the voltage decay is also following the same increasing trend as can be seen in Table 1.

Generally, at a fixed temperature, the slope is unchanged or independent of the applied voltage for a given activation-controlled self-discharge mechanism. In contrast, for a CR-controlled self-discharge, the slope is dependent upon the initial charging voltage and increases with voltage [30]. Therefore, at this stage, the observed change in the slope

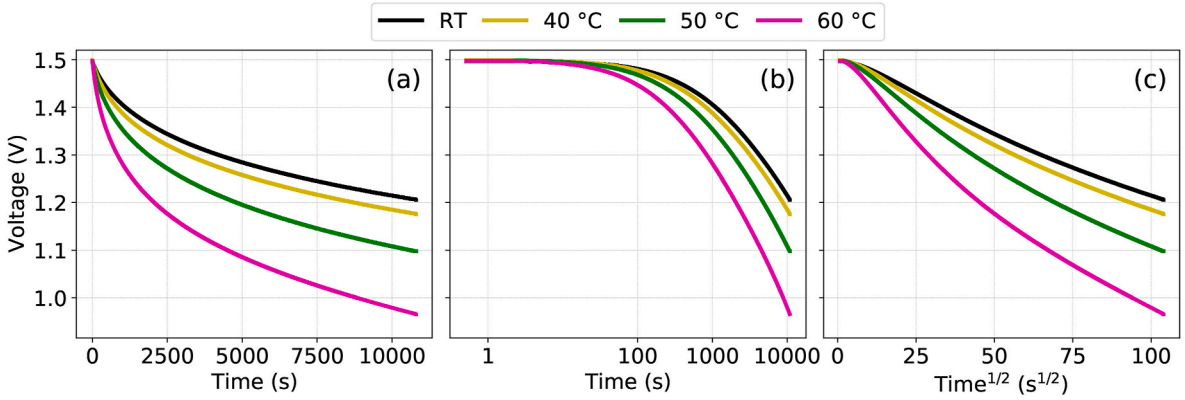

Fig. 1. Self-discharge of D_1 at different elevated temperatures: (a) voltage decay with time (t), (b) voltage decay as a function of time (t) in logarithmic scale, and (c) voltage decay with $t^{1/2}$.

Table 1
Increasing voltage-decay slope with temperature.

Temperature	RT	40 °C	50 °C	60 °C
dV/d [log t] (mV s^{-1})	83.4	88.6	106.8	132
dV/d [$t^{1/2}$] (mV s^{-1})	2.8	3	3.6	4.4

with temperature cannot be assigned solely to one of the mechanisms (CR- or activation-controlled). As a result, none of the mechanisms can be discarded or separated until the self-discharge profiles from different initial voltages at fixed temperatures are revealed, which is discussed further in section 3.3.

Fig. 1(c) shows a linear voltage decay with $t^{1/2}$, indicating the presence of diffusion-controlled self-discharge where the slope, traditionally, is associated with the initial concentration of the depolarizing species in the solution [21]. The observed diffusion-controlled self-discharge could also originate due to the presence of a low concentration

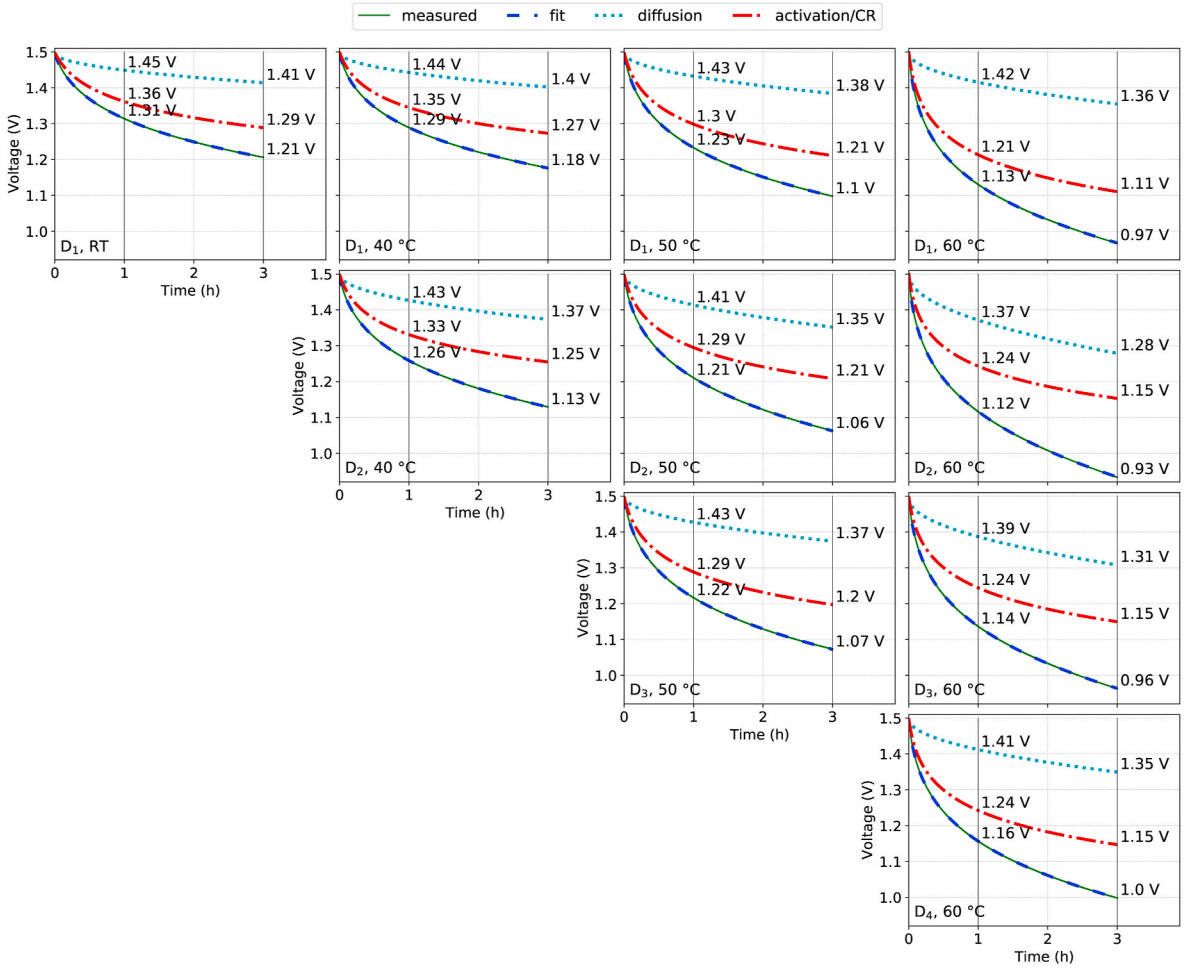

Fig. 2. Self-discharge profiles of D_1, D_2, D_3, and D_4 at different temperatures with experimental and fitted data.

of impurities like Fe, Al, Cu, and Ca, which were detected in the carbon material (YP-80 F) [49] used in this study as well. The similar behaviour with $t^{1/2}$ can also come from diffusion-limited CR, as stated and observed in previous studies [27,33,56]. With elevated temperatures, the voltage-decay slope is increasing (Table 1), indicating an enhanced initial ionic concentration, which is in agreement with observations in Ref. [21,54]. Chenglong Hao et al. [57] demonstrated that, due to the different nature of positive and negative ions, upon charging, the adsorption rate is different on the positive and negative electrodes, creating an ionic concentration gradient that is responsible for a fast diffusion process.

Therefore, from Fig. 1, it can be established that a mixed mechanism containing both diffusion and activation/CR is occurring in this system at a particular voltage of 1.5 V.

3.2. Identification of history dependence of self-discharge profile at elevated temperature and quantification of underlying mechanisms

Self-discharge behaviour is known to be influenced by operating history, temperature, charge duration, and charging current [53,57]. Since D_1 is operated at different temperatures (RT, 40 °C, 50 °C, and 60 °C) and allowed to equilibrate at least 4 h at each temperature step with multiple charge-discharge cycles, it cannot be excluded that the self-discharge behaviour at 60 °C could be affected by previous operation history. Therefore, it is of crucial practical significance to investigate the self-discharge behaviour with a systematic experimental procedure, involving specific temperature exposure (with controlled charging current and charge duration) to a series of devices.

Fig. 2 shows the effect of systematic temperature exposure on devices D_1 - D_4. The calculated voltage retention at the end of 3 h for all the devices can be found in Table S1. The observed increase in voltage loss with temperature can be considered linear for all the devices (Table S2). For instance, in the case of D_1, the increase in voltage loss is 2.5, 5, and 9 percental units with temperature increment from RT-40 °C, 40 °C–50 °C, and 50 °C–60 °C, respectively. A similar trend for the voltage loss is observed in D_2 and D_3 (Table S2).

In order to quantify the self-discharge mechanism of the devices, the measured data is fitted with the activation/CR and diffusion-controlled mechanism (Fig. 2). It can be observed that the voltage loss at 1.5 V for all the devices in the whole temperature range is accurately described with a combination of activation/CR and diffusion-controlled mechanisms. Fig. S3 shows the voltage loss contribution originating from both the mechanisms, and slight domination of activation/CR-controlled over diffusion-controlled mechanism is evident at 1.5 V for all the devices. The ratio of voltage loss originating from diffusion-over activation/CR-controlled mechanism lies between 0.4 and 0.6. The similar ratio of voltage loss for all the devices at a particular temperature suggests that the instant temperature strongly dictates the extent of voltage loss (higher loss at higher temperature) rather than the operating history of the devices. Therefore, the exposure of D_1 at RT, 40, and 50 °C does not strictly influence the underlying self-discharge mechanisms at 60 °C, but rather amplifies the voltage loss contribution from both the mechanisms. Individual variations are likely to originate from slightly different mass of the electrodes and the manual construction of the devices.

As a representative of all the devices, Fig. 3 shows the change of diffusion parameter and leakage resistance with increasing temperature for D_1. B.W. Ricketts and C. Ton-That [21] demonstrated that the diffusion parameter is a measure of excess ionic concentration in the double layer:

$$B = \frac{c_{EIC} \cdot \sqrt{D}}{C \cdot \sqrt{\pi}} \tag{6}$$

where B is the diffusion parameter, c_{EIC} is the excess ionic concentration in the double layer, D is the diffusion coefficient, and C is the interfacial series capacitance.

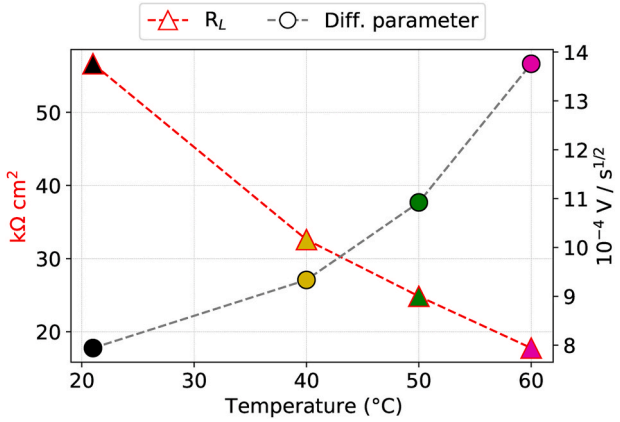

Fig. 3. Change of diffusion parameter and leakage resistance of D_1 with increasing temperature.

High temperature substantially increases the extent of the excess ionic concentration and strongly influences the diffusion parameter, causing a high self-discharge rate [21,54]. Similarly, it can be seen from Fig. 3 that the diffusion parameter (B) increases with temperature, and consequently, the leakage resistance decreases. Leakage resistance is calculated from the following relationship:

$$R_L = \frac{V}{I_L}\left(k\Omega \cdot cm^2\right) \tag{7}$$

where V is the maximum initial voltage after charging, I_L is the time-dependent leakage current required to maintain the set voltage (steady-state value, taken at the end of 2 h of potentiostatic hold), and R_L is the time-dependent leakage resistance.

3.3. Identifying the underlying self-discharge mechanisms

It is evident from the previous discussion that the diffusion-controlled mechanism is present in the observed self-discharge behaviour, but there is still uncertainty regarding the CR or activation-controlled mechanisms, given that both exhibit similar self-discharge profiles when plotted against log (t). One way to separate these two mechanisms is to observe the differences in the self-discharge profiles with different holding times. Fig. 4 shows the voltage decay of D_4 at RT and 60 °C with 120 min of holding and without any holding step after the initial charging to 1.5 V.

It can be seen that the voltage retention is higher with the holding step at both RT and 60 °C (Fig. 4 a, b) and that there is a noticeable change in the plateau length and slope of the voltage decay (Fig. 4 c, d). Generally, a self-discharge profile with an activation-controlled mechanism demonstrates no change in neither the plateau length, the final retained voltage, nor the slope upon repetitive charge and self-discharge cycle with different potentiostatic holding time. On the contrary, the self-discharge profile due to CR is significantly affected by the holding time after charging [30]. Inherently, CR occurs due to incomplete charging of the different RC subsystems in the porous carbon electrodes that results in a distributed potential and equilibrates during self-discharge. Therefore, with longer holding time or with a slow charging rate, more RC subsystems (related to more of the bulk material) get charged, and the voltage loss suffers less from the CR effect. Accordingly, the slopes of the linear voltage decay also decrease, and a higher voltage is retained with the subsequent holding step.

Due to the presence of the functional groups in the AC material, carbon oxidation is prone to happen, as evident at the initial cycles of the cyclic voltammogram (CV) with large anodic current (Fig. S2). However, with successive cycling, the oxidation wave decreases gradually as a result of less available surface reactive sites, and completely overlaps

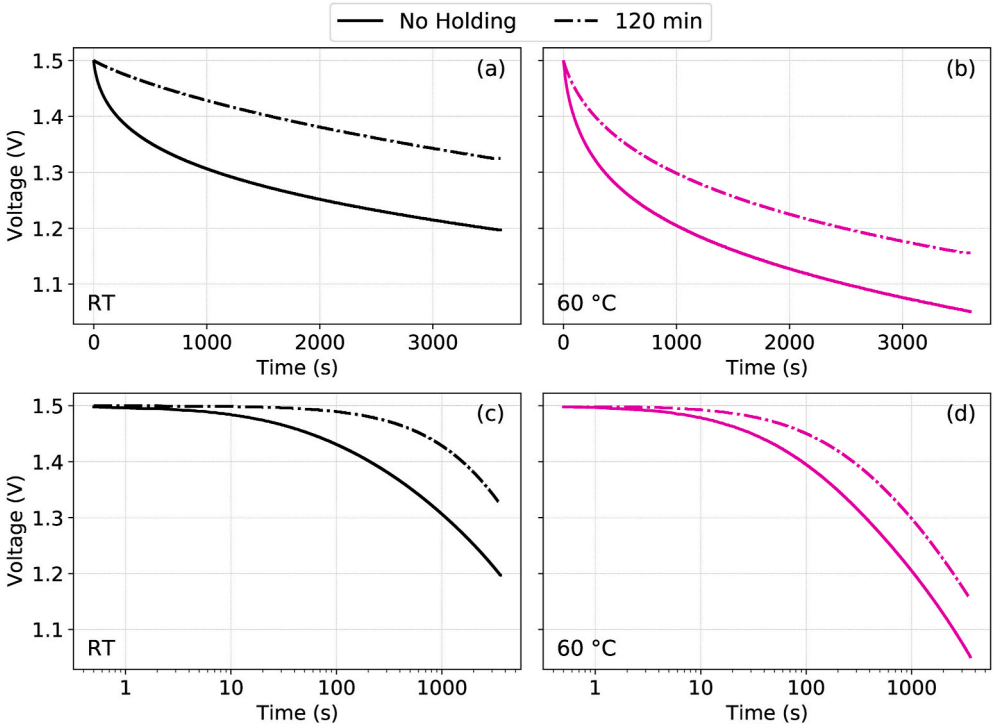

Fig. 4. Self-discharge after different holding time: (a, b) voltage decay with time (t), and (c, d) voltage decay as a function of time (t) in logarithmic scale.

at the end of cycling. This promotes a fully oxidized carbon surface and ensures a steady-state of the device. Regardless, if the activation-controlled reaction related to surface functional groups still contributes to the self-discharge, it would be recognized by the initial plateau length. With repetitive charge/self-discharge cycles, the plateau length will increase as a consequence of the depletion of available carbon surface oxides [58]. Fig. S4 shows the self-discharge profile at 1.5 V of all the 4 devices at 60 °C where D_1, D_2, D_3 and D_4 were cycled for 4, 3, 2 and 1 time, respectively, and no significant change in the plateau length can be observed. Therefore, the surface functional groups are likely to have a negligible impact on self-discharge behaviour in the current system.

This observation suggests that the self-discharge at 1.5 V is dominated by CR rather than by the activation-controlled mechanism. In order to further inspect the underlying self-discharge mechanisms at different polarizing voltages, Fig. 5(a) and 5(d) show the self-discharge behaviour of D_4 with different initial voltages, ranging from 1.0 to 1.5 V at both RT and 60 °C. No voltage holding step was performed prior to recording the V_{OC}.

The voltage loss is plotted against log (t) (Fig. 5 b, e) and $t^{1/2}$ (Fig. 5 c, f) to recognize the underlying mechanisms. It can be noticed from Fig. 5 and Table 2 that the slopes of the declining voltages strongly depend on the initial voltages both at RT and 60 °C. The increasing voltage-decay slope with increasing polarization voltage is again in good agreement with the CR controlled self-discharge mechanism rather than the

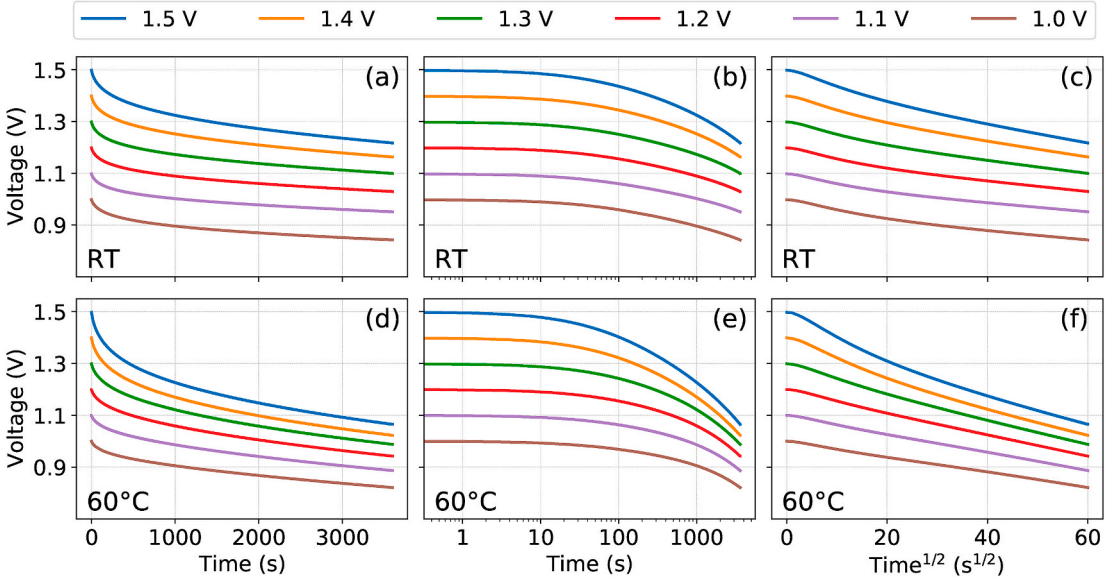

Fig. 5. Self-discharge behaviour at different initial voltages at RT and 60 °C: (a, d) voltage decay with time, (b, e) voltage decay as a function of time in logarithmic scale, and (c, f) voltage decay with $t^{1/2}$.

Table 2
Increasing voltage-decay slope with different initial voltage at RT and 60 °C.

	RT		60 °C	
Voltage (V)	dV/d [log t] (mV s^{-1})	dV/d [$t^{1/2}$] (mV s^{-1})	dV/d [log t] (mV s^{-1})	dV/d [$t^{1/2}$] (mV s^{-1})
1.5	96.2	3.5	145.5	5.4
1.4	81.4	3	133.2	4.9
1.3	69.1	2.5	123.8	4.6
1.2	56.7	2.1	111.2	4.1
1.1	48.1	1.8	97.2	3.6
1.0	47.4	1.7	83.9	3.1

activation-controlled mechanism [30].

Similarly, the linear drop in the voltage in Fig. 5(c) and 5(f) demonstrates that the diffusion-controlled self-discharge is also present in the entire range of initial voltages, and the increasing slope of voltage decay in the diffusion profile with temperature indicates an enhanced diffusion process. Based on the above pieces of evidence, a mixed mechanism containing CR and diffusion is occurring at the entire polarizing voltage range at both RT and 60 °C.

In order to quantify the contributions from each mechanism, Fig. 6 displays the fitting of the measured self-discharge data with the diffusion-controlled model and CR-controlled model. The fitting accurately describes the measured data.

It can be seen that with increasing initial voltage, the voltage retention decreases at both RT and 60 °C. For instance, at 1.0 V initial voltage, 85%, and 82% voltage is retained at the end of 1 h self-discharge at RT and 60 °C respectively, while at 1.5 V initial voltage, the voltage retention is calculated to be 80% at RT and 70% at 60 °C. Voltage retention for all the nominal voltages can be found in Table S3. The higher initial voltage at 60 °C suffers from voltage loss significantly more compared to the lower initial voltage at the same temperature.

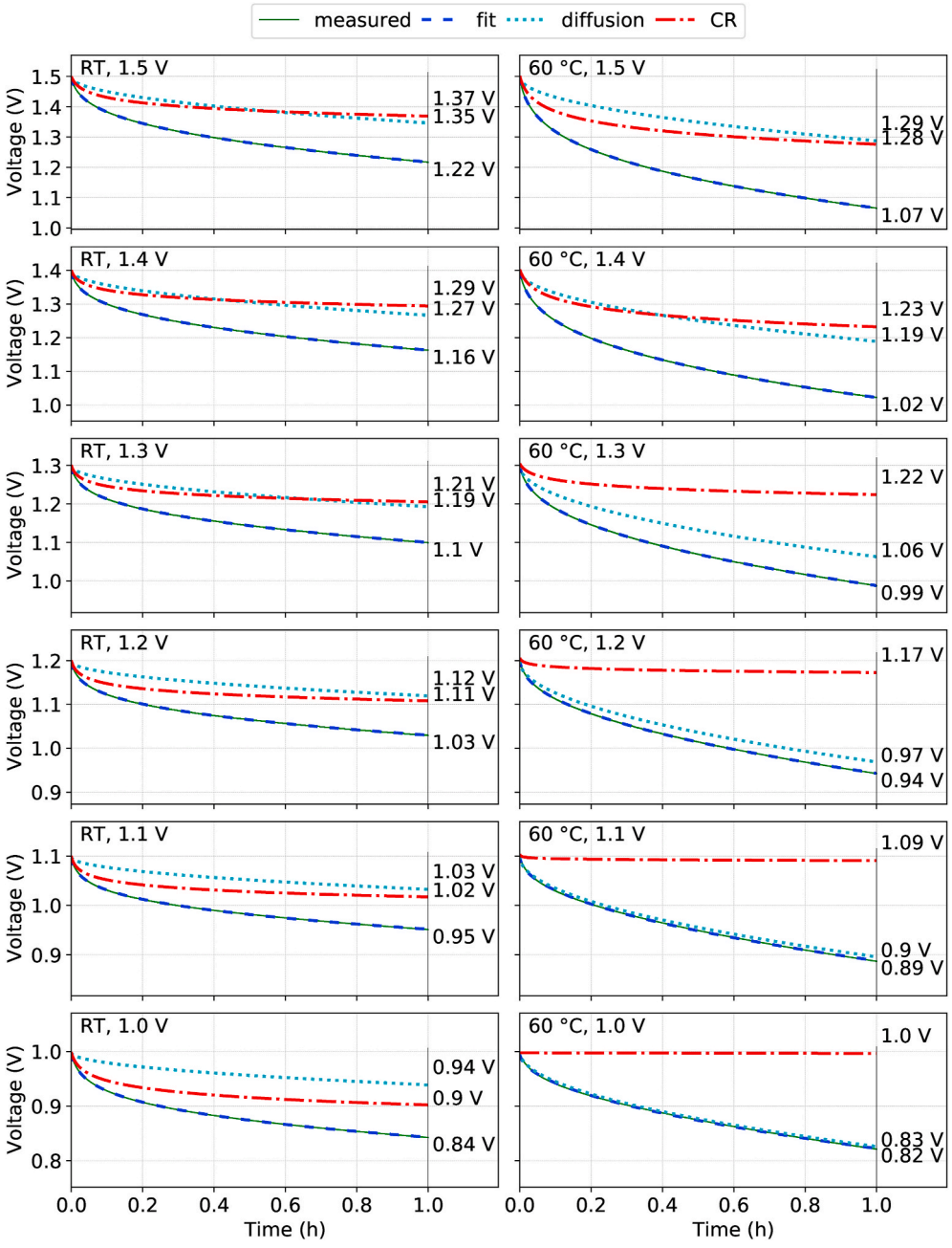

Fig. 6. Time dependence of the voltage decay of D_4 at different initial voltages with experimental data and fitted data.

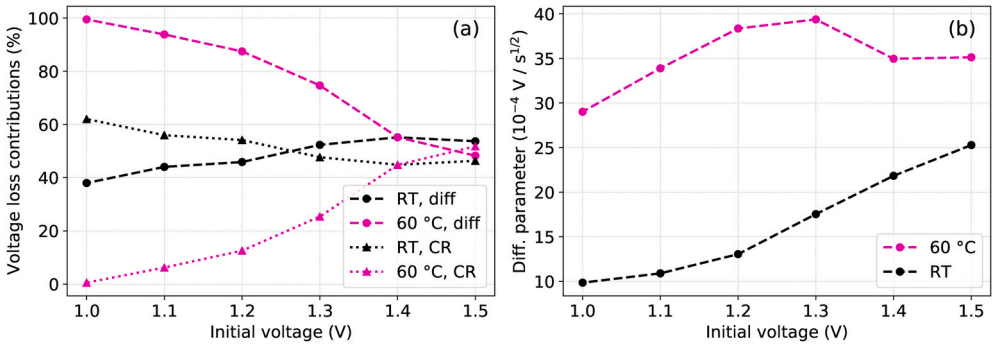

Fig. 7. (a) Voltage loss contribution from CR and diffusion mechanisms, and (b) diffusion parameter at different initial voltages at RT and 60 °C.

Moreover, two competing self-discharge mechanisms can be noticed at different initial voltages, especially at 60 °C, as visualized in Fig. 7(a). An interesting trend is observed where the voltage decay for the device at RT has a similar contribution from diffusion and CR, although until 1.2 V voltage loss due to CR is slightly higher, while from 1.3 V upward the contribution from diffusion becomes somewhat larger. On the other hand, at 60 °C, a strong dominance of diffusion can be noticed until 1.2 V, but it gradually decreases with increasing voltage, and eventually, the contribution from CR becomes slightly higher at 1.5 V.

As there is no potentiostatic holding step involved before self-discharge starts, the contribution from a CR mechanism is expected, due to unequal potential distribution in the electrodes. The diffusion mechanism is also be part of the self-discharge as a result of the concentration gradient originating from different adsorption rates of cations and anions. The similar contributions from both the mechanisms at RT is expected, considering that the kinetics of the system is not changing substantially with an increasing initial voltage. On the other hand, at elevated temperature (60 °C), the kinetics within the system would significantly change, and most likely, upon charging, there would be an excess of ionic concentration close to the electrodes. In an open circuit condition, the excess ions try to diffuse to an equilibrium state by reaching towards the bulk electrolyte. Consequently, the voltage loss observed is dominated by a diffusion-controlled self-discharge mechanism.

The lower contribution of the CR in the voltage loss at 60 °C can be explained in terms of two factors. Firstly, due to the change of ionic liquid property at elevated temperatures. For instance, the resistivity of an IL butyltrimethylammonium bis(trifluromethylsulfonyl)imide (BTM) decreases from 476 Ω cm at 25 °C to 17.5 Ω cm at 200 °C [59]. Similarly, the viscosity of the EMIM Ac electrolyte decreases by a factor of 32 from RT to 120 °C [60]. Generally, in porous electrodes, the electrolyte solution resistance is the limiting factor for the migration of the ions in the pores. Therefore, the increased ionic conductivity of the electrolyte ensures a more complete charging among different RC subsystems, which lowers the overall τ_{RC}. Secondly, due to the influence of the magnitude of the charging current used to reach the initial voltage. A low constant current of 0.05 A g^{-1} promotes a more uniform distribution of ions across the electrolyte and the charges across the electrodes. Therefore, at elevated temperature, the combination of both lowered τ_{RC} and low charging current suppresses the CR effect in the voltage decay under the open-circuit configuration. However, this applies only up to a certain voltage. The magnitude of thermal agitation of the electrolyte is more pronounced at a high initial voltage, creating an unbalanced ionic distribution and more unstable double layers. Consequently, the contribution from the CR mechanism increases with increasing initial voltage as can be seen around 1.5 V.

Fig. 7(b) shows the change of diffusion parameter with increasing initial voltage for both RT and 60 °C. In general, an increase in the diffusion parameter can be noticed with the elevated temperature at all initial voltages. A slight drop in the diffusion parameter at 1.4 V and 1.5 V further confirms that the CR mechanism approaches to take over the self-discharge process at higher initial voltages.

3.4. Elevated temperature influence on leakage current and impedance characteristic

Fig. 8 shows the change of leakage current of D_1, recorded during the potentiostatic holding period of 2 h after charging to the initial voltage of 1.5 V. The leakage current corresponds to the charge readjustment in the porous electrodes and is essentially equivalent to the self-discharge current.

It can be seen that the leakage current is high in the beginning and reaches a steady value with time. The value of steady-state leakage current is higher at higher temperature. As the self-discharge is a kinetic process, the temperature variation naturally influences the self-discharge behaviour of the system. The observed change is strongly associated with an activation energy. The temperature influence on leakage current (or self-discharge current) follows the Arrhenius relation, which plays a dominant role in classical chemical kinetics and can be expressed as follows:

$$I_L = A \exp\left(-\frac{E_a}{RT}\right) \tag{8}$$

The dependence of the rate constant can be expressed over a wide range of temperature through equation (8) where A is a pre-exponential factor, E_a is the activation energy, R is the universal gas constant (8.31451 J mol^{-1} K^{-1}), T is the temperature in Kelvin and I_L is the leakage current. If the ln (I_L) holds a linear relation with $1/T$, then the slope is equivalent to $-E_a/R$, from which the activation energy can be calculated. Consequently, Fig. 8(b) illustrates the logarithm of the normalized leakage current over the reciprocal of the temperature. It can be seen that the plot exhibits a straight line with a slope of (−2.5). From this value, the activation energy is calculated to be 21 ± 1 kJ mol^{-1}. This value is very close to the activation energy related to diffusion-controlled processes (16–20 kJ mol^{-1}), whereas an activation energy of 40–80 kJ mol^{-1} is representative of an activation-controlled process [2]. In this regard, the activation energy associated with this device strongly indicates that the self-discharge mechanism is driven by a diffusion-controlled mechanism in addition to the CR effect.

As the extent of the CR effect depends on τ_{RC}, it is worthwhile to investigate the change of τ_{RC} with elevated temperature. The decrease of the electronic conductivity of the AC electrode due to elevated temperature is negligible compared to the increase of ionic conductivity of EMIM Ac electrolyte. Therefore, the observed change in τ_{RC} is mostly related to the resistance of the electrolyte. In this regard, EIS can provide a detailed mapping of the ionic motion, such as bulk electrolyte conductivity at high frequency and ionic conductivity inside the pores at low frequency.

Fig. 8 (c) shows the Nyquist plot at different temperatures. It can be noticed that the equivalent series resistance (ESR), the 1st intersection

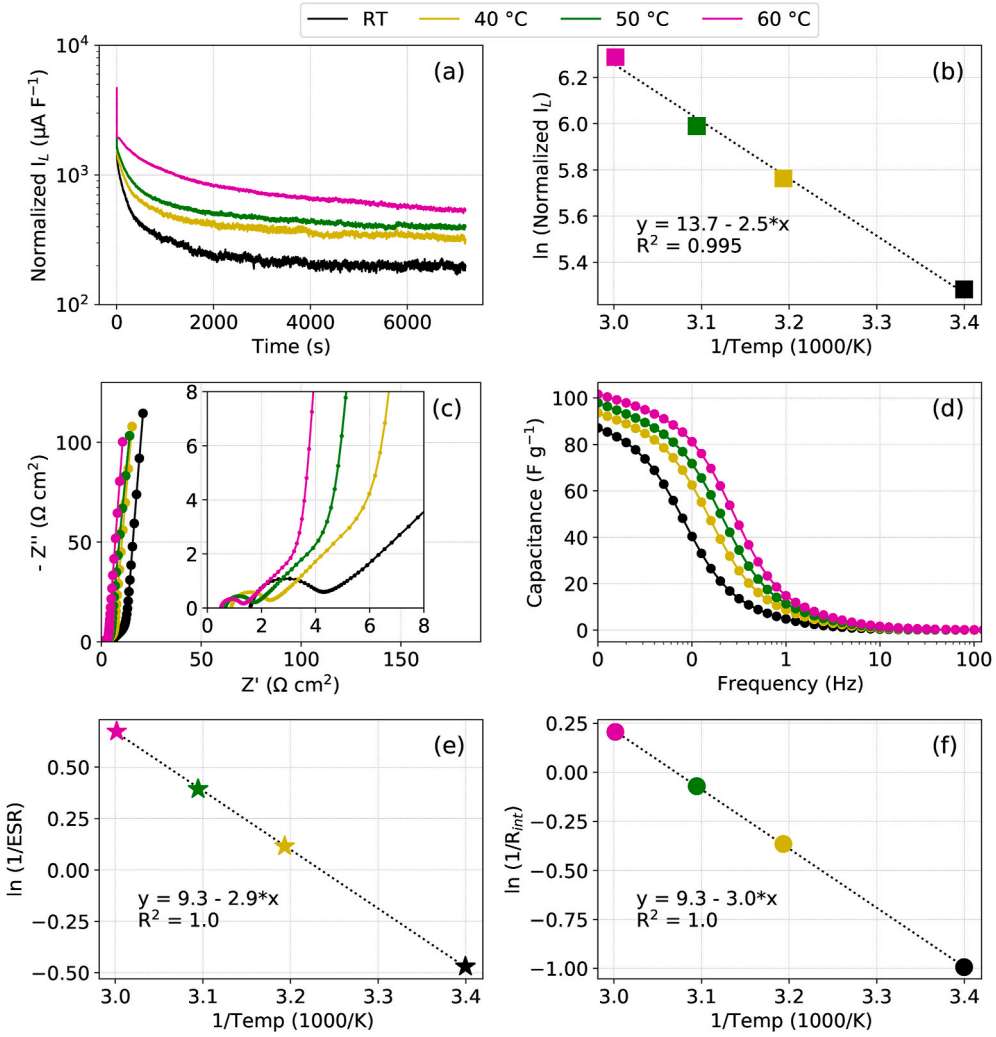

Fig. 8. (a) Leakage current of D_1 at different temperatures, (b) Arrhenius plot of leakage current from RT to 60 °C, Impedance behaviour at different temperature (c) Nyquist plot (d) Capacitance variation with frequency, (e) variation of ESR and (f) variation of R_{int} in the form of Arrhenius plot.

point of the semicircle in the Z′ axis at highest frequency, is decreasing with elevated temperature. As the ESR mostly arises from the electrolyte solution resistance, a decreased ESR value corresponds to increased ionic conductivity of the electrolyte. The 2nd intersection point of the semicircle corresponding to the interfacial resistance (R_{int}), is also decreasing with elevated temperature. Finally, the resistance in the lowest frequency, named diffusion resistance, $R_d = Z'(0.01\,Hz) - (ESR + R_{int})$, falls from 17 to 9 Ω cm^2 from RT to 60 °C. Fig. 8 (e) and (f) demonstrate the adaptation of the Arrhenius plot in terms of ESR and R_{int} at different temperatures and the corresponding activation energy from the slope is calculated to be 24 ± 1 and 25 ± 1 kJ mol^{-1} respectively. Both the plots exhibit a straight line, which is representative of the direct influence of the temperature variation. Therefore, the observed decrease in resistance in the whole frequency region is a result of improved ion diffusivity and kinetics related to thermally activated behaviour of electrolyte ions. Fig. 8 (d) shows the equivalent capacitance variation with elevated temperature. Naturally, the equivalent capacitance increases with the temperature at the lowest frequency. Nevertheless, the decrease in solution resistivity is far more significant. Therefore, the overall τ_{RC} decreases considerably with elevated temperature and the extent of self-discharge due to CR mechanism is less prominent, at least for the lower initial voltages.

4. Conclusion

The reported study focuses on the influence of the elevated temperature on the self-discharge behaviour of a carbon-based supercapacitor containing an ionic liquid (EMIM Ac) electrolyte. Measurements are taken at RT, 40, 50, and 60 °C from initial voltages of 1.0–1.5 V.

A systematic temperature exposure on four devices indicated that the increased self-discharge rate is predominantly influenced by the instant temperature exposure rather than the operating history of the devices. In the present system, the voltage loss due to ohmic leakage and activation-controlled Faradaic processes were ruled out, based on the results of mathematical models with governing equations of different self-discharge mechanisms, as well as activation energy calculation. A mixed mechanism of charge redistribution and diffusion is therefore considered to be responsible for the observed voltage decay. At an elevated temperature of 60 °C, the diffusion-controlled mechanism dominates at lower initial voltages over charge redistribution effect, while at RT both mechanisms contribute similarly. The reduced contribution from charge redistribution at 60 °C in the lower initial voltage is due to a decreased RC time constant (τ_{RC}), which is confirmed by the impedance measurements.

The observed mechanism is allegedly applicable in other ionic liquid-based supercapacitors as the properties of ionic liquid electrolytes change in a similar fashion with elevated temperatures. The insights into

the underlying self-discharge mechanisms of ionic liquid-based supercapacitors can be applied to address the uncertainty in the performance and increase reliability during elevated temperature operation.

CRediT authorship contribution statement

Mazharul Haque: Conceptualization, Methodology, Investigation, Visualization, Data curation, Writing - original draft, Writing - review & editing, Formal analysis. **Qi Li:** Conceptualization, Methodology, Writing - review & editing, Resources. **Cristina Rigato:** Visualization, Writing - review & editing, Formal analysis. **Azega Rajaras:** Data curation, Investigation. **Anderson D. Smith:** Writing - review & editing. **Per Lundgren:** Writing - review & editing, Supervision, Project administration. **Peter Enoksson:** Supervision, Project administration, Funding acquisition, Writing - review & editing.

Declaration of competing interest

The authors declare that they have no known competing financial interests or personal relationships that could have appeared to influence the work reported in this paper.

Acknowledgments

The authors gratefully acknowledge Vinnova UDI project Miniaturized self-powered industrial sensor systems using energy harvesting technologies-Energy Supply Toolkit (2017–03725), Architectures for High-Power Radars (2017–04869), Chalmers Area of Advance project Microelectronic Energy Storage systems for Integration Alongside Harvesters (MESSIAH), Chalmers University of Technology, and The Wallenberg Wood Science Center (WWSC) funded by Knut and Alice Wallenberg Foundation for financial support of this work.

Appendix A. Supplementary data

Supplementary data to this article can be found online at https://doi.org/10.1016/j.jpowsour.2020.229328.

References

[1] R. Kotz, M. Carlen, Electrochim. Acta 45 (2000) 2483–2498.
[2] B.E. Conway, W. Pell, T. Liu, J. Power Sources 65 (1997) 53–59.
[3] A. Du Pasquier, I. Plitz, S. Menocal, G. Amatucci, J. Power Sources 115 (2003) 171–178.
[4] Q. Li, M. Haque, V. Kuzmenko, N. Ramani, P. Lundgren, A.D. Smith, P. Enoksson, J. Power Sources 348 (2017) 219–228.
[5] C. Zhong, Y. Deng, W. Hu, J. Qiao, L. Zhang, J. Zhang, Chem. Soc. Rev. 44 (2015) 7484–7539.
[6] X. Zang, C. Shen, M. Sanghadasa, L. Lin, ChemElectroChem 6 (2019) 976–988.
[7] F. Béguin, V. Presser, A. Balducci, E. Frackowiak, Adv. Mater. 26 (2014) 2219–2251.
[8] K. Fic, G. Lota, M. Meller, E. Frackowiak, Energy Environ. Sci. 5 (2012) 5842–5850.
[9] B. Akinwolemiwa, C. Peng, G.Z. Chen, J. Electrochem. Soc. 162 (2015) A5054–A5059.
[10] F. Markoulidis, C. Lei, C. Lekakou, D. Duff, S. Khalil, B. Martorana, I. Cannavaro, Carbon 68 (2014) 58–66.
[11] C. Liu, Z. Yu, D. Neff, A. Zhamu, B.Z. Jang, Nano Lett. 10 (2010) 4863–4868.
[12] V. Augustyn, P. Simon, B. Dunn, Energy Environ. Sci. 7 (2014) 1597–1614.
[13] L. Yu, G.Z. Chen, J. Power Sources 326 (2016) 604–612.
[14] J. Zhang, X. Zhao, ChemSusChem 5 (2012) 818–841.
[15] W. Wang, S. Guo, I. Lee, K. Ahmed, J. Zhong, Z. Favors, F. Zaera, M. Ozkan, C. S. Ozkan, Sci. Rep. 4 (2014) 4452.
[16] M.R. Lukatskaya, B. Dunn, Y. Gogotsi, Nat. Commun. 7 (2016) 12647.
[17] A. Jagadale, X. Zhou, R. Xiong, D.P. Dubal, J. Xu, S. Yang, Energy Storage Mater 19 (2019) 314–329.
[18] J. Niu, B.E. Conway, W.G. Pell, J. Power Sources 135 (2004) 332–343.
[19] J. Niu, W.G. Pell, B.E. Conway, J. Power Sources 156 (2006) 725–740.
[20] R. de Levie, Electrochim. Acta 8 (1963) 751–780.
[21] B.W. Ricketts, C. Ton-That, J. Power Sources 89 (2000) 64–69.
[22] B. Pillay, J. Newman, J. Electrochem. Soc. 143 (1996) 1806.
[23] K. Kierzek, E. Frackowiak, G. Lota, G. Gryglewicz, J. Machnikowski, Electrochim. Acta 49 (2004) 515–523.
[24] H.A. Andreas, K. Lussier, A.M. Oickle, J. Power Sources 187 (2009) 275–283.
[25] S. Kazaryan, G. Kharisov, S. Litvinenko, V. Kogan, J. Electrochem. Soc. 154 (2007) A751–A759.
[26] S. Kazaryan, S. Litvinenko, G. Kharisov, J. Electrochem. Soc. 155 (2008) A464–A473.
[27] H.A. Andreas, J. Electrochem. Soc. 162 (2015) A5047–A5053.
[28] J.M. Black, H.A. Andreas, J. Phys. Chem. C 114 (2010) 12030–12038.
[29] H. Yang, Y. Zhang, J. Power Sources 273 (2015) 223–236.
[30] J. Black, H.A. Andreas, Electrochim. Acta 54 (2009) 3568–3574.
[31] J. Chmiola, G. Yushin, Y. Gogotsi, C. Portet, P. Simon, P.-L. Taberna, Science 313 (2006) 1760–1763.
[32] S. Fletcher, V.J. Black, I. Kirkpatrick, J. Solid State Electrochem. 18 (2014) 1377–1387.
[33] H.A. Andreas, J.M. Black, A.A. Oickle, Electrochim. Acta 140 (2014) 116–124.
[34] S.-E. Chun, B. Evanko, X. Wang, D. Vonlanthen, X. Ji, G.D. Stucky, S.W. Boettcher, Nat. Commun. 6 (2015) 7818.
[35] S. Ban, J. Zhang, L. Zhang, K. Tsay, D. Song, X. Zou, Electrochim. Acta 90 (2013) 542–549.
[36] H. Olsson, M. Strømme, L. Nyholm, M. Sjödin, J. Phys. Chem. C 118 (2014) 29643–29649.
[37] J.W. Graydon, M. Panjehshahi, D.W. Kirk, J. Power Sources 245 (2014) 822–829.
[38] B. Wang, J. Maciá-Agulló, D. Prendiville, X. Zheng, D. Liu, Y. Zhang, S. Boettcher, X. Ji, G. Stucky, J. Electrochem. Soc. 161 (2014) A1090–A1093.
[39] G. Shul, D. Bélanger, Phys. Chem. Chem. Phys. 18 (2016) 19137–19145.
[40] L. García-Cruz, P. Ratajczak, J. Iniesta, V. Montiel, F. Béguin, Electrochim. Acta 202 (2016) 66–72.
[41] T. Xiong, Z.G. Yu, W.S.V. Lee, J. Xue, ChemSusChem 11 (2018) 3307–3314.
[42] Q. Zhang, J.P. Rong, D.S. Ma, B.Q. Wei, Energy Environ. Sci. 4 (2011) 2152–2159.
[43] Q. Zhang, J. Rong, B. Wei, RSC Adv. 1 (2011) 989–994.
[44] Q. Zhang, C. Cai, J. Qin, B. Wei, Nano Energy 4 (2014) 14–22.
[45] M. Armand, F. Endres, D.R. MacFarlane, H. Ohno, B. Scrosati, Nat. Mater. 8 (2009) 621–629.
[46] G. Xiong, A. Kundu, T.S. Fisher, Thermal Effects in Supercapacitors, Springer, New York, 2015.
[47] B.E. Conway, Electrochemical Supercapacitors: Scientific Fundamentals and Technological Applications, Kluwer academic: plenum press, New York, 1999.
[48] N. Handa, T. Sugimoto, M. Yamagata, M. Kikuta, M. Kono, M. Ishikawa, J. Power Sources 185 (2008) 1585–1588.
[49] A. Laheäär, A. Arenillas, F. Béguin, J. Power Sources 396 (2018) 220–229.
[50] F. Soavi, C. Arbizzani, M. Mastragostino, J. Appl. Electrochem. 44 (2014) 491–496.
[51] M. Haque, Q. Li, A.D. Smith, V. Kuzmenko, E. Köhler, P. Lundgren, P. Enoksson, Electrochim. Acta 263 (2018) 249–260.
[52] K. Ge, G. Liu, Chem. Commun. 55 (2019) 7167–7170.
[53] J. Kowal, E. Avaroglu, F. Chamekh, A. S'enfelds, T. Thien, D. Wijaya, D.U. Sauer, J. Power Sources 196 (2011) 573–579.
[54] L.H. Hess, L. Wittscher, A. Balducci, Phys. Chem. Chem. Phys. 21 (2019) 9089–9097.
[55] J. Black, H.A. Andreas, J. Power Sources 195 (2010) 929–935.
[56] T. Liu, W. Pell, B. Conway, Electrochim. Acta 42 (1997) 3541–3552.
[57] C. Hao, X. Wang, Y. Yin, Z. You, J. Electron. Mater. 45 (2016) 2160–2171.
[58] A.M. Oickle, J. Tom, H.A. Andreas, Carbon 110 (2016) 232–242.
[59] S. Fletcher, V.J. Black, I. Kirkpatrick, T.S. Varley, J. Solid State Electrochem. 17 (2013) 327–337.
[60] S. Fendt, S. Padmanabhan, H.W. Blanch, J.M. Prausnitz, J. Chem. Eng. Data 56 (2011) 31–34.